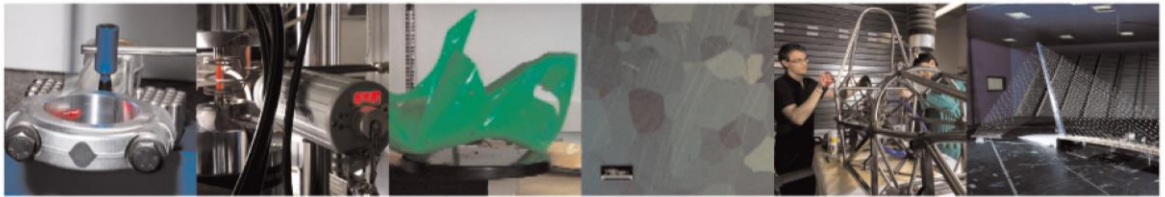




**POLITECNICO**  
MILANO 1863

DIPARTIMENTO DI MECCANICA



## In-line monitoring of focus shift by kerf width detection with coaxial thermal imaging during laser cutting

Ema Vasileska, Matteo Pacher, Barbara Previtali

This is a post-peer-review, pre-copyedit version of an article published in INTERNATIONAL JOURNAL, ADVANCED MANUFACTURING TECHNOLOGY. The final authenticated version is available online at: <http://dx.doi.org/10.1007/s00170-021-07893-8>

This content is provided under [CC BY-NC-ND 4.0](https://creativecommons.org/licenses/by-nc-nd/4.0/) license



IN-LINE MONITORING OF FOCUS SHIFT BY KERF WIDTH DETECTION WITH COAXIAL THERMAL IMAGING  
DURING LASER CUTTING

Ema Vasileska<sup>a\*</sup>, Matteo Pacher<sup>b</sup>, Barbara Previtali<sup>a</sup>

<sup>a</sup>Department of Mechanical Engineering, Politecnico di Milano, Via La Masa 1, 20156 Milan, Italy

<sup>b</sup>Adige S.P.A.,BLMGROUP, Via per Barco 11, 38056, Levico Terme (TN), Italy

\*Corresponding author, vasileskaema@gmail.com

<b>IN-LINE MONITORING OF FOCUS SHIFT BY KERF WIDTH DETECTION WITH COAXIAL THERMAL IMAGING DURING LASER CUTTING</b>	<b>3</b>
<b>Abstract</b>	<b>3</b>
<b>1 Introduction</b>	<b>3</b>
1.1 Motivation	3
1.2 State of art	4
1.3 Aims	5
<b>2 Proposed method for in-line monitoring of focus shift</b>	<b>6</b>
2.1 Theoretical model	6
2.2 Image analyses algorithm	7
2.3 Threshold calibration	8
<b>3 Material, equipment, and experimentation</b>	<b>9</b>
3.1 Material	9
3.2 Equipment	9
3.3 Experimental design, execution, and measurements	10
<b>4 Results and discussion</b>	<b>13</b>
4.1 Measured experimental $W_{top}$	13
4.2 Image analyses algorithm calibration	15
4.3 Process modelling	17
<b>5 Conclusions</b>	<b>18</b>
<b>Acknowledgements</b>	<b>19</b>
<b>Declarations</b>	<b>19</b>
Funding	19
Conflict of interest	19
Availability of data and material	19
Code availability	19
<b>References</b>	<b>19</b>

# In-line monitoring of focus shift by kerf width detection with coaxial thermal imaging during laser cutting

## Abstract

Nowadays industrial laser cutting systems employ a fixed set of process parameters throughout the cut of the same workpiece, which results in a good compromise between maximum productivity and surface quality. The process parameters are commonly set by trial-and-error experiments carried out on different materials and thicknesses or less frequently by physical modelling. However, the final cut quality is not constant even though the process parameters are kept fixed due to degradation of the initial status of the laser cutting system. One of the common issues in the laser cutting process is the local heating of the optical components due to contamination and/or high powers commonly employed, which cause shifting of the focus position. This can worsen the cutting-edge quality, and even result with loss of cut. Therefore, the online measurement of the position of focus is a requirement for a consistent process. An empirical method used in the industrial practice for initially setting and successively examining and adjusting the focus position is to measure the kerf width of a straight-line cut performed with constant process parameters. This paper proposes an algorithm to monitor the kerf width and yield the estimated focus position in real-time during the cutting process. The kerf width is observed during the process with a coaxial camera module mounted on the laser head which monitors the thermal interaction between the laser beam and the material. An image processing algorithm was developed for extracting the kerf width from the acquired images, and the algorithm parameters were experimentally calibrated such that the extracted value of the kerf width matches with its physical measure. To understand the influence of the focus position on the cutting kerf, an experimental campaign was conducted and subsequently a regression model was fitted. The real-time monitoring and computation of the kerf width and its correlation to the focus position give the opportunity for a closed-loop control of the focus shift, that would eventually lead to a gain of process stability and repeatability.

Keywords: laser cutting, thermal lensing, focus shifting, coaxial process monitoring, cutting kerf monitoring

## 1 Introduction

### 1.1 Motivation

Created from the words “Light Amplification by Stimulated Emission of Radiation”, lasers have been an embodiment of efficiency and quality in materials processing since their advent in the sixties. They offered an entirely new form of energy which in turn enabled many previously unfeasible applications, often replacing mechanical methods. Able to heat, melt and even vaporize material, lasers represent the ideal medium for channeling intense but controllable energy.

So far, the most popular use of lasers is for cutting in both macro and micro applications [1][2]. The process works by directing the laser beam through an optical chain, ending with a focusing lens and protective window, to the workpiece. The combination of the energy beam concentrated by the focusing lens and pressure of the assist gas ejected by the nozzle creates the cutting action. The material melts, burns, vaporizes, or is blown away by the jet of gas, generating a removed volume of material defined as the *kerf*, and leaving an edge with a high-quality surface finish. The laser optics and CNC (Computer Numerical Control) are used to direct and then to move the laser beam generated onto the material, resulting with a continuous cut. Cut quality depends upon the proper selection of process parameters, since all cutting parameters have a significant influence on the resulting surface quality [3][4]. In general, cutting parameters are adjusted and tuned based on trial-and-error experiments or more rarely on

empirical and physical models to provide the desired quality of the cut and maximized productivity [5][6][7]. Among others, the focus position regulates the spot diameter and consequently the release of the energy onto the workpiece and co-operates with the nozzle diameter and stand-off distance to properly direct the gas jet into the cutting kerf.

Maintaining the focus position at the optimal value results in delivering correct power and energy density at the focal plane, which is crucial for the repeatability of laser-cut parameters and producing consistent edge quality [3]. However, a fraction of the laser emission is absorbed in optical elements, leading to thermal loading on the optics, particularly when high-brilliance and high-power laser beams are used. Contaminations on the optical surfaces further enhance their absorption. The local heating of the optical components due to thermal load generated on the lens and its coating can distort the optical elements resulting with a phenomenon known as thermal lensing [8]. The consequence of the phenomenon is a shift of the focus position value from the optimal conditions, altering the power density input on the workpiece. Resultantly, the edge quality of the workpiece is highly affected leading to cutting edge defects or even un-cuts if it is abundantly eminent, degrading the process stability and repeatability [9][10].

## 1.2 State of art

To minimize and/or compensate the problem of heating and consequent thermal deformation of the lens, different approaches have been presented in the literature. Firstly, to avoid heating, lenses are optimized to not absorb or totally reflect the laser radiation; furthermore, they can be cooled with internal refrigerant circuits. Secondly, to monitor the degradation over time, sensors are mounted on the lens or in its vicinity, such as thermopiles, thermocouples or ultrasound probes [11][12][13]. Thirdly, different strategies for compensation of the degradation have been studied. Active compensation of the thermally induced lenses (like adaptive mirrors based on piezoelectric actuators) can be adopted [14][15]. The drawback is the increase of the devices incorporated in the optical chain and consequent complexity. Passive compensation using optical lens materials with negative temperature coefficient of the refractive index is a satisfactory solution that is being studied and implemented [16][17][18].

In those cases, where the lens holders and optical chain of the machine cannot host sensors that directly measure the contamination and thermal heating, sensing the focus shift as a consequence of the thermal lensing is a necessity for avoiding or attenuating its effects. Moreover, sensing the focus shift allows to monitor the state of the overall optics as well as the occurrence of unpredictable events that might worsen the beam quality.

The focus position must be measured or estimated to control performance and provide consistent process conditions over time. In the literature direct and indirect methods for quantifying the focus position are presented.

The direct methods comprise of adopting measuring tools for monitoring the beam properties, such as beam waist diameter, focus position, BPP, complete caustics over up to four Rayleigh lengths [19]. The reference technique for directly observing the phenomenon is measuring the caustic beam with the principle of serial scanning, as the scanning tool like PRIMES HP-MSM-HB [PRIMES GmbH, Pfungstadt, Germany]. This measurement setup is adopted in a research conducted by Hemmerich et al. studying ways to compensate focus shift effects in industrial laser welding [20]. The same tool is used by Abt et al. to measure with high temporal resolution the step function response of the laser induced focus shift of beam forming optics [21]. In the experiment performed by K. R. Mann et al. different F-theta lenses are thermally loaded by laser irradiation, and the thermal beam waist displacement is determined by caustic measurement according to ISO 11146 [16]. The serial scanning method is very useful because it measures the focused beam properties in correspondence of the workpiece position and with the laser beam at the process power. However, due to the measurement method and time as well as

the apparatus size, this direct approach cannot be used in-line during cutting but only during ad hoc campaigns of beam qualification.

Conversely, other in-line methods for direct measurements of the focus shift make use of auxiliary reference laser beam that passes through all the optical elements in the process laser beam path. Therefore, focus shift of the laser beam also affects the reference beam. The focus of the reference beam can be measured online during processing, thus making accessible also the focus of the laser beam. These methods were already under investigation by the late 1970s, when Stamper et al. performs one of the first experiments for accurately monitoring small laser focus shift [22]. Negel et al. proposed the use of a bundle of astigmatic measurement beams following the same optical path as the processing welding beam; the focal position depends on the measurement beams projected ellipses over the workpiece [23]. Reitemeyer et al. investigated the focus shifting in laser welding, proposing a novel method for measuring the focus shift by determining the focus position with CCD camera of a second beam uncoupled from the laser beam without additional optical elements in the beam path [24].

On the other side, indirect methods present opportunity for monitoring the focus displacement while cutting by means of monitoring process quantities linked to the focal position. The signal detection is used either to document the quality characteristics or to regulate the machining process. Quantifying the focus position by monitoring a correlated quantity gives opportunity for an indirect in-process measurement of the quality of cut, since if compared with a set point, it allows to monitor the degradation of the performance in time and therefore determine control actions for avoiding defects.

By measuring the temperature distribution of the process zone with a coaxial high-temperature camera, Haferkamp et al. correlated the shape of the observed cutting kerf with the focus position, concluding that an effective control of the focal position is possible by controlling the shape of the temperature field [25]. Moreover, by irradiating the observed sheet surface and acquiring images of the cutting kerf with a coaxial high-speed camera, Thombsen et al. proved that the shift in the focus position imposes variation of the width of the cutting kerf [26]. Weingartner analyzed the radiation spectrum from the laser – material interaction zone with a spectrometer and correlated the observed phenomenon to distance between the molten zone and the focusing lens [27]. Bordatchev et al. analyzed the acoustic emissions generated by the laser-material interaction and studied the effect of the focus position on the properties of the measured signals, providing statistical classification of actual focus position which can be used for process diagnostics and control [28].

Already adopted industrial solution for focus shift avoidance in real systems is presented by Messer Cutting Systems (Rödermark, Germany). The scattered laser light coming from the cutting process is analyzed using a telecentric lens assembly on a CCD camera. Each individual pixel in a single line of the CCD camera detects the scattered light as a measuring point of intensity in the beam profile. From these measurements, the beam and beam-quality parameters can be calculated according to ISO-13694 and ISO-11146 standards.

### 1.3 Aims

One possibility to process stability is to evaluate in real-time the focus position with a monitoring module and later compensate possible errors with a feedback control system. This study presents a method for monitoring the laser cutting process estimating in real-time the focus position and indicating when focus shift takes place. With a low cost Near-Infrared (NIR) camera mounted coaxially on the laser head, the geometry of the thermal interaction between the laser beam and the material, thus the cutting kerf, can be monitored. As aforementioned, the width of the cutting kerf is significantly influenced by the focus position. With an appropriate image processing algorithm, the kerf width can be extracted from the camera frames and then correlated to the position of the focus through a process model elaborated in this study. The process model is calibrated by an ad hoc experimentation, whose data has been partially used to calibrate the image algorithm and partially used as confirmation runs of the proposed regression model.

## 2 Proposed method for in-line monitoring of focus shift

### 2.1 Theoretical model

The lumped capacity thermal model developed by Steen [33] proves the proportionality of the kerf width  $W_{top}$  to several process parameters:

$$W_{top} = \frac{P}{v \cdot T \cdot \Delta h_V}$$

Eq. 1

where  $P$  is the laser power,  $v$  is the cutting speed,  $T$  is the cutting plate thickness, and  $\Delta h_V$  is the necessary increase in volumetric enthalpy as the characteristic thermodynamic function of state. The volumetric need of energy  $\Delta h_{V,N2}$  when nitrogen is used as assisting gas for cutting can be estimated with the caloric equation of state:

$$\Delta h_{V,N2} = \rho \cdot [C_{P,S} \cdot (\vartheta_{m.p.} - \vartheta_0) + \Delta h_{S/L} + m' \cdot \Delta h_{L/V}]$$

Eq. 2

where  $\rho$  is the material density,  $C_{P,S}$  is the average of the specific heat capacity of the solid material in the range between the melting point temperature  $\vartheta_{m.p.}$  and the ambient temperature  $\vartheta_0$ ,  $\Delta h_{S/L}$  is the specific enthalpy of the phase transition from solid to liquid state (fusion),  $m'$  is the fraction of melt vaporized and  $\Delta h_{L/V}$  is the specific enthalpy of the phase transition from liquid to vapor state (vaporization).

From Eq. 1 it is evident that the kerf width is depending on the  $P$ ,  $v$  and  $\Delta h_V$ . When the material properties and the workpiece thickness as well as the process parameters do not change along the cutting operation, the kerf width is expected to be constant, unless the focus position and consequently the spot diameter on the material surface  $d_s$  vary. In fact, the main hypothesis behind the simplified model in Eq. 1 is the constancy of the beam properties and relative position to the workpiece, i.e., the spot diameter  $d_s$  and focus position  $f$ . The spot diameter  $d_s$  and kerf width  $W_{top}$  are proportional, with  $W_{top}$  being slightly larger than  $d_s$  due to thermal effects of the laser energy input on the material, as depicted on Fig. 1. Given these hypotheses, the proportionality between  $W_{top}$  and  $d_s$  is introduced with a purely geometrical caustic model which neglects the material-laser interaction:

$$W_{top} \propto d_s = \sqrt{d_0^2 + \theta^2 \cdot f^2}$$

Eq. 3

where  $\theta$  is the divergence angle,  $d_0$  is the waist diameter and  $f$  is the focus position. The focus position  $f$  is defined as the distance from the top surface of the plate to the beam focal plane. As can be seen in Fig. 1, the focus position  $f$  is calculated as the difference between the stand-off distance ( $SOD$ ) and the distance from the nozzle tip to the focal point (denoted with  $p_f$  in this study):

$$f = SOD - p_f$$

Eq. 4

where the  $SOD$  is defined as the distance between the tip of the nozzle and the material plate.

Consequently, negative value of focus position corresponds to a focal point found below the top plate surface, while positive if it is above. Moreover, the divergence angle  $\theta$  is derived from the following relation:

$$\theta = \frac{4 \cdot \lambda}{\pi \cdot d_0} \cdot M^2$$

Eq. 5

where  $M^2$  is the beam quality factor,  $\lambda$  is the laser emission wavelength and  $d_0$  the waist diameter [32].

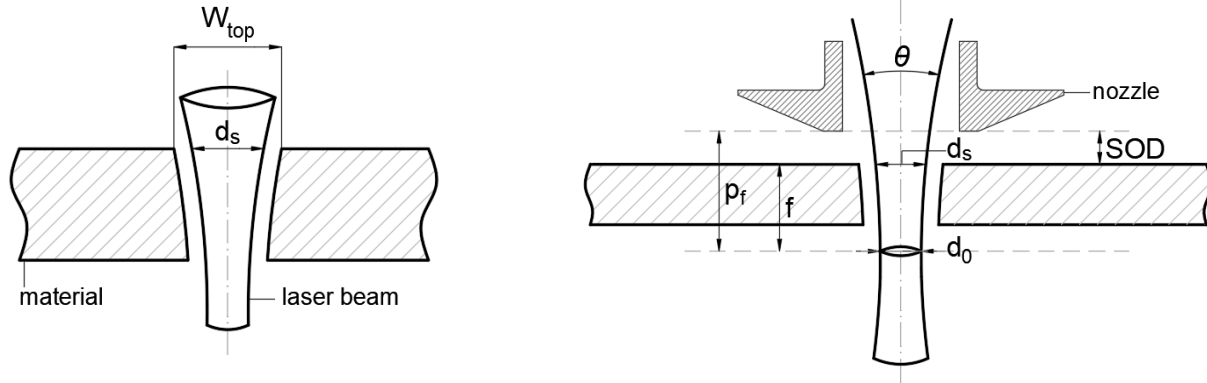


Fig. 1: Cross section view of the laser beam profile defining the used distances.

From Eq. 3 and Eq. 4 it is determined that the  $W_{top}$  relates to the beam caustic quantities which are fixed parameters and varies only as a function of the focus point  $p_f$ . Therefore, when the focus shifting occurs, the focus position  $f$  is differing, which directly influences the width of the generated kerf.

The proposed new method assumes  $W_{top}$  as indirect quantity revealing drift in the focus position due to thermal lensing or any other event that could change the laser beam position during the laser cutting operation. The relationship of  $W_{top}$  with respect to all the other process parameters is assumed to be known a-priori before cutting. In this way variations of  $W_{top}$  due to events different than focus shifting, such as transitory in speed during intricate path, are already embedded in the a-priori correlation between speed and power.

## 2.2 Image analyses algorithm

The new method makes use of a commercial coaxial camera setup to acquire in-line thermal images of the advancing kerf that is analyzed and processed to estimate the actual  $W_{top}$  in case of laser fusion cutting with nitrogen. The setup is connected directly onto the machine working head, thus looking through the cutting head to directly observe the zone of interaction of laser beam and material. The reference frame of the setup is moving together with the process zone such that it follows the on-going process, allowing the sensor to always monitor the direct laser-material interaction.

For estimating the value of the kerf width, the image analysis algorithm consisted of binarizing the images of the molten pool, extracting the kerf, and calculating the kerf width.

Considering the original grayscale image as a matrix  $I \in \mathbb{R}_{n \times m}$ , with  $m, n \in \mathbb{N}$  being the number of rows and columns respectively, each element of the matrix is a pixel with grey level value  $g_{i,j} \in [0,255]$ , where value of 0 represents a black pixel and value of 255 is a white pixel. Each pixel can be represented as a vector  $p_k \in N_3, k \in [1, m \cdot n]$  defined as:

$$p_k = \begin{pmatrix} i \\ j \\ g_{i,j} \end{pmatrix}$$

Eq. 6

where  $i \in [1, m], j \in [1, n]$  are the rows and columns indexes of matrix  $I$  identifying the pixel and  $g_{i,j}$  is its grey level. Therefore, each image can be considered as a dataset composed by points  $p_k$  that represents the two spatial coordinates of a pixel and its intensity value.

Firstly, a 2-D Gaussian smoothing filter with standard deviation set to 2 was used due to the white noise which was perceived in the images, which followed the Gaussian distribution. Next, segmenting the image to consider only the reduced area of the image where the cutting operation is preserved is of great



computational interest. Finally, the image is binarized by applying a hard thresholding algorithm for separating the solid metal and the cutting region. To correctly distinguish between solid heated zone and actual molten material, a proper threshold value needs to be chosen. Hard thresholding principle is defined as [29]:

$$\tilde{g}_{i,j} = \begin{cases} 1 & g_{i,j} \geq C \\ 0 & g_{i,j} < C \end{cases}$$

Eq. 7

where  $g_{i,j}$  is the grey level of the original image  $I$ ,  $\tilde{g}_{i,j}$  is pixel value of the binary image,  $I_{bin}$ , resulting from the operation and  $C$  is the value of the threshold. After this procedure, all the light contributions coming from heated solid are set to 0, while all the light coming from the kerf itself is set to 1, and it results with the kerf appearing as a white blob on a black background. The calibration procedure of the threshold value is thoroughly explained in Subchapter 2.3.

The last phase of the image processing algorithm is extracting the parameter of interest looking for certain geometries and removing the noise in order to identify the kerf indicators. After the thresholding, all the connected regions are established in the binary image, and the kerf is identified as the region with the maximum area and minimum blob centroid (the blob with the minimum distance from the image center). Following the kerf recognition, it is rotated as a function of the angle between the machine axis and the camera, such that the estimated width of the kerf is found as the maximum sum of white pixels along horizontal direction multiplied by the spatial resolution [mm]. The kerf is extracted, and the kerf width value is calculated from every frame acquired from the NIR camera during the cutting process. The value of the estimated kerf width from the process images is denoted with  $W_{est}$ . An example of the kerf width extraction for a single frame is shown on Fig. 2, where the kerf width is denoted with  $W_{est}$ .

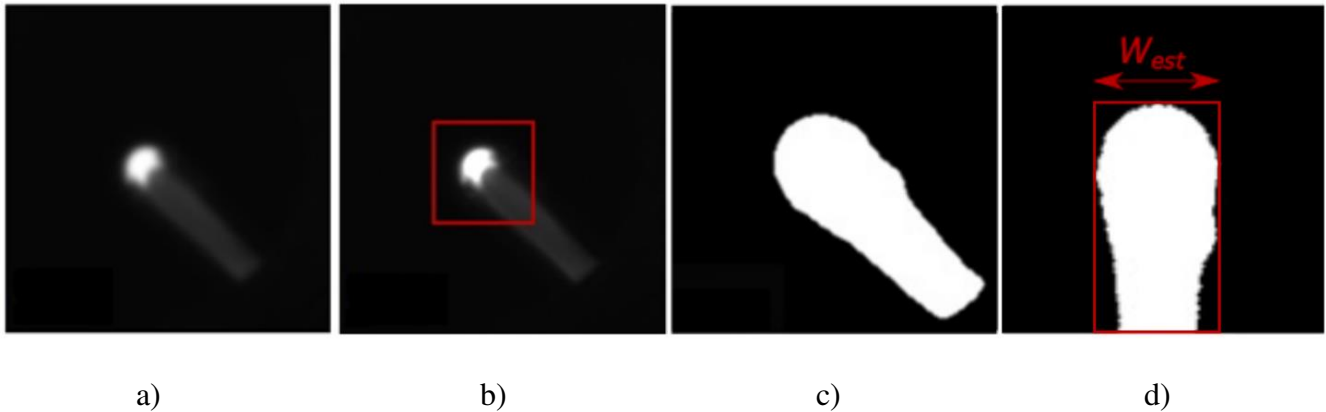


Fig. 2: Steps in image processing algorithm: a) Filtered image  $I$ ; b) Area of segmentation; c) Binarized image  $I_{bin}$ ; d) Final cropped and rotated image for extracting the width  $W_{est}$  ( $C = 10$ ; workpiece thickness = 3 mm)

### 2.3 Threshold calibration

For an accurate calculation of the kerf width from the process emission images, the image processing algorithm in Eq. 7 was calibrated by choosing the optimal value of the threshold  $C$  for binarizing the NIR images. The optimal threshold is defined by comparing the measured  $W_{top}$  with the  $W_{est}$  found with the certain threshold value and calculating the total error  $e_{TOT}$  between them. The calculation of  $e_{TOT}$  is defined with the following equation:

$$e_{TOT} = \frac{1}{M} \sum_{k=1}^M \frac{1}{N} \sum_{j=1}^N \left( W_{top}(k) - W_{est}(k,j) \right)^2$$

Eq. 8

where  $k$  indicates the number of the cut and varies from 1 to  $M$  ( $M$  is number of total cuts) and  $j$  is the image index (from 1 to  $N$  for each cut number  $k$ ). The single measured  $W_{top}$  value of cut  $k$  is compared with the  $W_{est}$  extracted by each image belonging to the same cut  $k$ , whose value depends on the threshold  $C$ . Dividing for  $N$  and  $M$  a single error value is computed which considers the effect of all images and samples in the same way. The value of the error depends on the threshold  $C$ . By repeating the analysis with different  $C$  values, the optimal threshold is found as the one that gives the lowest error value. A schematic representation of the procedure for threshold calibration is shown on Fig. 3.

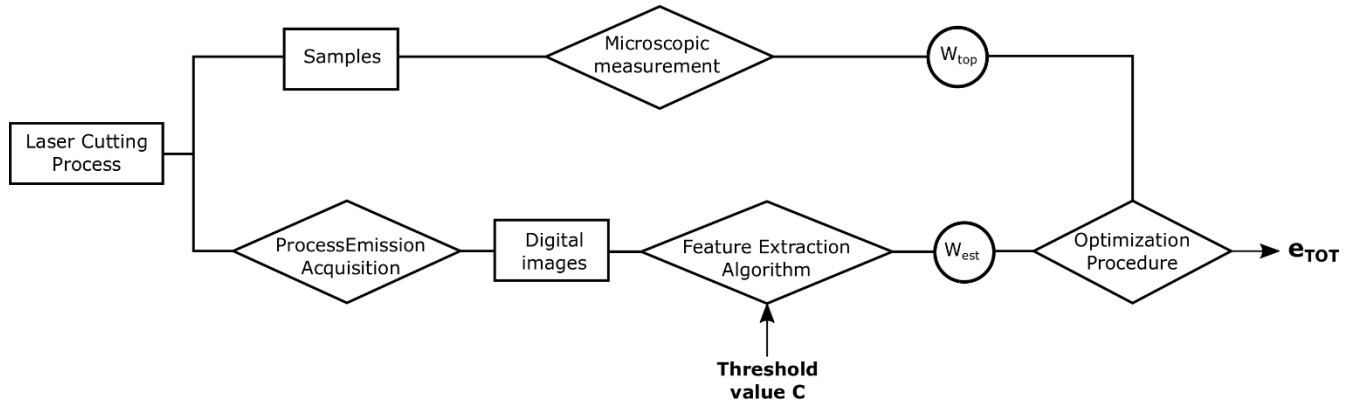


Fig. 3: Schematic representation of the optimization procedure for finding the optimal threshold ( $C$ ) value

### 3 Material, equipment, and experimentation

#### 3.1 Material

Material considered for all the experimental campaign was stainless steel AISI 304 in the form of metal sheet. Different thicknesses were examined in the range of 3 - 8 mm. Influence of material type is not covered in this study.

#### 3.2 Equipment

##### 3.2.1 Laser cutting system

The machine employed in the experimental campaign was a customized version of the LC5 cutting machine (Adige-SYS S.p.A. BLMGroup, Levico Terme, Italy) which can cut both metal sheets and tubes. It has a maximum working area of 3000 mm × 1500 mm for sheet cutting and can cut tubes with external diameter up to 125 mm. The cutting is performed in open air environment in the enclosed machine chamber.

The laser source is a high-power fiber laser source, with maximum deliverable power of up to 6 kW (YLS-6000-CUT, IPG Photonics Corp., Oxford, Massachusetts). The transport fiber is a graded-index optical fiber with a core diameter of 100 μm. The cutting head (HPSSL, Precitec GmbH & Co., Gaggenau, Germany) provides customization for monitoring purposes. The focal lengths of the processing and collimation lenses are equal to 200 mm and 100 mm, respectively.

Table 1: Main characteristics of the laser cutting system

Parameter	Value
Laser emission wavelength, $\lambda$	1070 nm
Max. laser power, $P_{max}$	6 kW
Beam quality factor, $M^2$	11.7
Beam diameter on focal plane, $d_0$	210 $\mu\text{m}$
Divergence angle, $\theta$	0.08 rad

### 3.2.2 Monitoring setup

The monitoring optical chain implemented on the machine head is demonstrated in Fig. 4. The chosen camera sensor is an industrial CMOS camera based on Si photodetectors with a sensitivity between 350-1000 nm. To observe the variations of the kerf geometry with sufficient accuracy in different cutting conditions and different thicknesses, the camera lens was selected such that Field of View (FOV) of 2 mm x 2 mm and spatial resolution equal to 9.6  $\mu\text{m}/\text{px}$  is obtained [30].

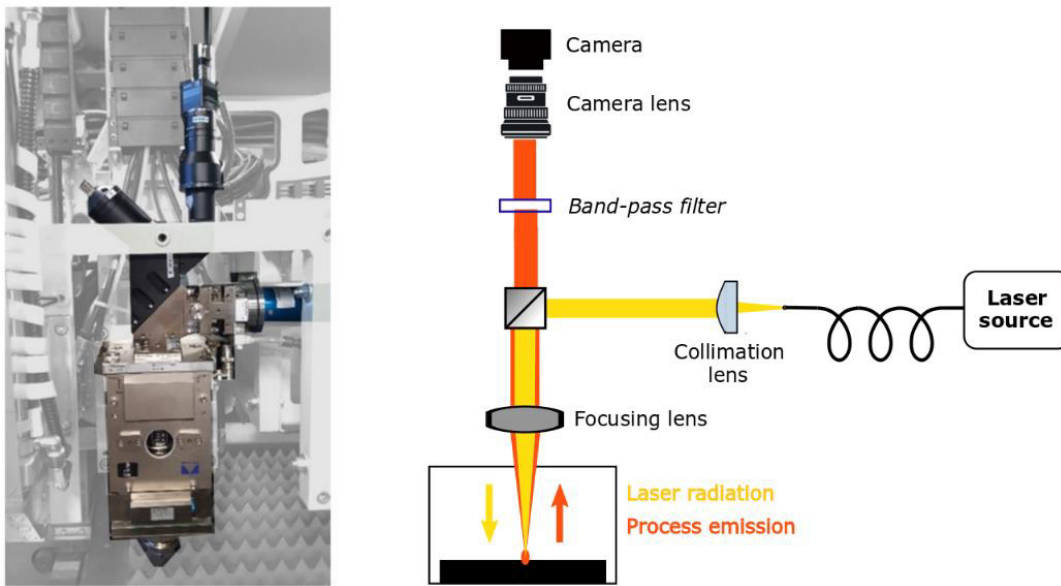


Fig. 4: Image of the monitoring module installed on the machine (left) and scheme of the optical chain (right).

As the laser interacts with the material and creates the melting point, the process thermal emission along with the laser light back-reflection are transmitted back to the sensor, and the radiation of interest which provides direct and reliable information about the on-going process is the NIR radiation compatible with the observable spectrum of the camera.

### 3.3 Experimental design, execution, and measurements

The cutting process employs a set of parameters delivering best quality cut with maximized productivity. The optimal parameters combination is selected according to the cutting thickness, such that the nominal speed depends on the maximum power achievable for time and cost efficiency. The parameters used in the experiment are presented on Table 2.

Table 2: Fixed cutting parameters employed in the experiment (abbreviations according to Fig. 1)

Thickness	Power	Velocity	Pressure	Stand-off distance	Nozzle diameter	Nominal nozzle tip-focal point distance
$T$	$P$	$v$	$p$	$SOD$	-	$p_f$
[mm]	[kW]	[mm/min]	[bar]	[mm]	[mm]	[mm]
3	6	7500	16	0,5	1,8	3,50
4	6	5500	19	0,7	2,3	4,70
5	6	4500	16	0,7	2,3	5,70
8	6	3500	18	0,5	2,5	7,00

The employed assist gas was N<sub>2</sub>, where the gas pressure depends on the cutting thickness. The laser power was maintained constant for all the conditions at the highest value aiming to maximize the manufacturing productivity, therefore the delivered beam power was not a variable parameter. The nominal cutting speed based on the material thickness was confirmed in a preliminary experiment to result in a dross-free cut.

The impact of the thermal properties of the material and the process parameters on the generated kerf width is eliminated by keeping them constant throughout the cut, and therefore only the  $p_f$  will be influencing factor to the kerf width as shown on Eq. 3 and Eq. 4. When using an inert gas, the focal point as the point with maximum energy density should be positioned closer to the lower plate surface. In this way the focused laser beam brings the base metal quickly to a molten state and creates a proper cut channel, allowing the inert gas to expel the liquefied material and form a cut surface with no dross adherence [3]. Having defined nominal sets of process parameters, in the preliminary experiment a nominal  $p_f$  distance was found per thickness which results with optimal part quality. The range in which the focus position will shift provided the employed optical chain and process parameters was estimated with the equation for steady-state focus shift developed by Miyamoto et al. [31]:

$$\Delta f = \left( \frac{2 \cdot A \cdot P \cdot f_{foc}^2}{\pi \cdot K \cdot D_L^2} \right) \cdot \frac{dn}{dT}$$

Eq. 9

where  $A$  is the beam absorptance of lens,  $K$  is the thermal conductivity,  $D_L$  is the diameter of the incident beam,  $f_{foc}$  is the focus length,  $n$  is the refractive index and  $dn/dT$  is the refractive index change with temperature. The parameters were selected based on the lens material ZnS and its properties for the lens [32], and a focus shift in the order of approximately 1.6 mm was derived. Therefore  $\pm 1$  mm was experimented for obtaining the theoretically computed range of the overall focus position variation.

Table 3: Values used for calculation of focus shift range in Eq. 9, considering ZnS lens material

	Abbreviations	Units	Value
Laser Power	$P$	[W]	6000
Focus length	$f_{foc}$	[mm]	200
Lens Absorptivity	$A$	[m <sup>-1</sup> ]	0.04
Thermal conductivity of the lens	$K$	[W/cm/ °C]	0.272
Diameter of incident beam	$D_L$	[mm]	20
Temperature change of refractive index	$dn/dT$	[/°C]	4.20E-05

Two experiments were performed. The data from the first experiment were elaborated to calibrate the threshold value  $C$  for binarization in the image analyses algorithm (see Eq. 7). Additionally, the measured kerf width of the specimens provided confirmation of the focus position significance for the kerf width variation and statistical rejection of the material thickness as a variable parameter. The latter experiment

was performed to estimate and later validate a regression model between the nozzle tip – focal point distance  $p_f$  and the generated kerf width  $W_{est}$ .

The experiment aiming to empirically assess the relationship between  $W_{est}$  and the focus position  $p_f$  consists of a sequence of straight-line cuts, each equal to 70 mm, each one performed with a certain combination of parameters depending on the thickness. For modelling the influence of the focal position and plate thickness on the kerf width, four different thicknesses were considered: 3, 4, 5 and 8 mm. Densely distributed thicknesses were cut (3, 4, 5 mm) as well as plate of 8 mm for a more distributed data set and a general solution. The only variable parameter per thickness was the nozzle – focal point distance  $p_f$  which was manually changed before every cut to resemble the focus shift phenomenon, in a range of variation proper of the expected focus shift. Per each thickness, 9 different values of  $p_f$  were investigated, such that each cut was realized with one value of  $p_f$  and then replicated 3 times. Based on nominal  $p_f$  (highlighted with grey color in Table 4), different cut conditions were realized in a range of +/- 1 mm with respect to the nominal one with a step of 0.25 mm. Therefore, a total of 27 cuts per thickness were performed, thus 108 cuts in total, run in a random order to obtain a dataset which is robust to non-controllable effects that can be time-variant or depend on the order of the measurement. The cuts were then collected in 3 rectangular samples containing 9 straight-line cuts each per every thickness as shown on Fig. 5, resulting with 12 rectangular samples in total (108 straight-line cuts).

Table 4: Varied cutting parameters employed in the experiment for model estimation

Thickness [T]	[mm]	3	4	5	8
Nozzle – focal plane distance [ $p_f$ ]	[mm]	4,50	5,70	6,70	8,00
		4,25	5,45	6,45	7,75
		4,00	5,20	6,20	7,50
		3,75	4,95	5,95	7,25
		3,50	4,70	5,70	7,00
		3,25	4,45	5,45	6,75
		3,00	4,20	5,20	6,50
		2,75	3,95	4,95	6,25
		2,50	3,70	4,70	6,00

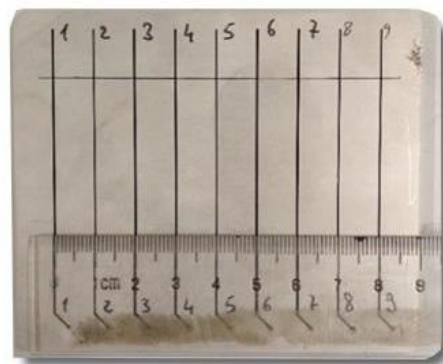


Fig. 5: Rectangular sample collecting 9 straight-line cuts

In the experiment for threshold calibration, additional 162 cuts were performed, where three different thicknesses were considered: 3, 5 and 8mm, and three different nozzle – focal point distances  $p_f$  were studied per thickness summarized on Table 5. Each condition was replicated 18 times, resulting with 54

cuts per thickness, and 162 cuts in total. Cuts were then collected in rectangular samples for simpler later analysis; each sample contained 9 cuts where one cut equals 70 mm.

In both experiments and in all experimented cutting conditions, the material was cut through the whole thickness with just a single pass.

Table 5: Varied cutting parameters employed in the experiment for threshold calibration

Thickness [T]	[mm]	3	5	8
Nozzle – focal plane distance [ $p_f$ ]	[mm]	2,40	3,60	5,00
		3,00	4,50	6,25
		3,60	5,40	7,50

The coaxial monitoring setup was continually employed in the experimental campaign for acquiring thermal images from the processing zone in order to have information related to the generated kerf.

### 3.3.1 Measurement apparatus

The Mitutoyo Quick Vision QV-ELF202 (Mitutoyo Corporation, Kanagawa, Japan) optical microscope is a non-contact dimension measurement system. Equipped with a CCD camera, it is used to acquire and measure the generated kerf width.

Varying kerf widths were created depending on the focus position employed for performing the corresponding cut, which was clearly observable also by eye. To quantify the value of the generated kerf width, a measurement procedure was conducted employing a measurement software tool implemented into Mitutoyo microscope; a line in the contrast region is created and the distance to opposite contrast point is the dimension of interest.

Three measures were acquired of each cut at three different positions (denoted with a, b and c on Fig. 6). These measures are appointed as  $W_{top}$ .

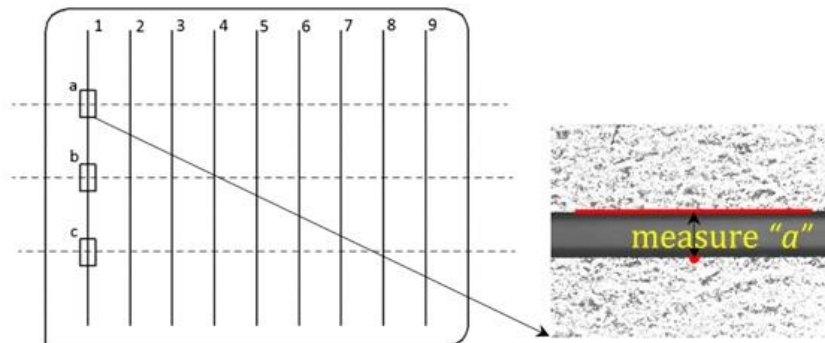


Fig. 6: Measurement of  $W_{top}$ : three measures (a, b, c) of one cut are acquired with optical microscope

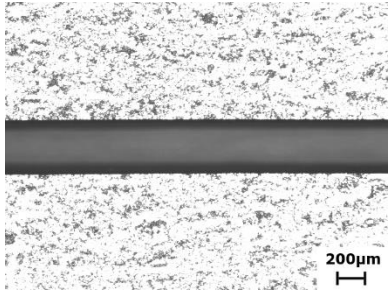
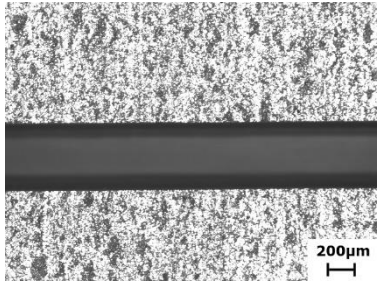
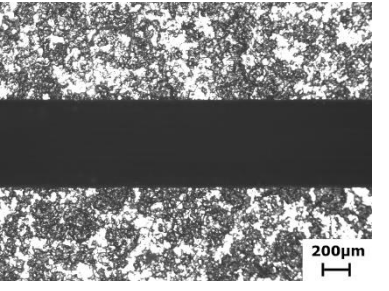
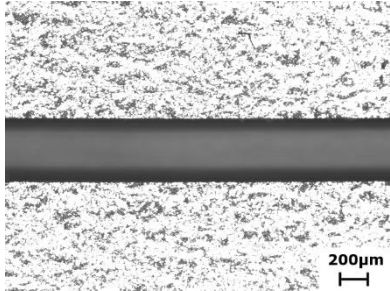
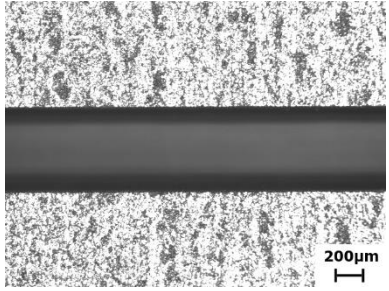
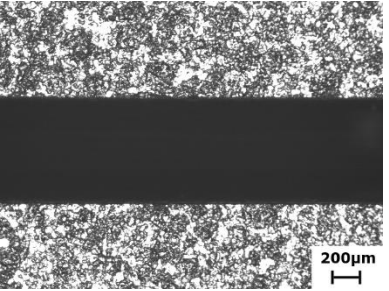
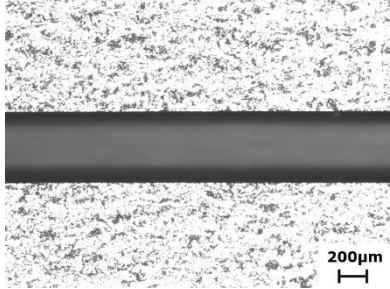
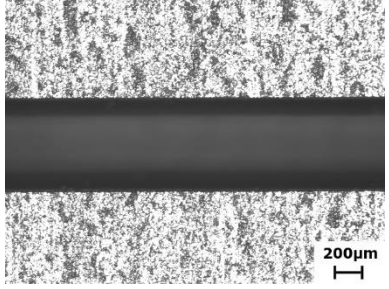
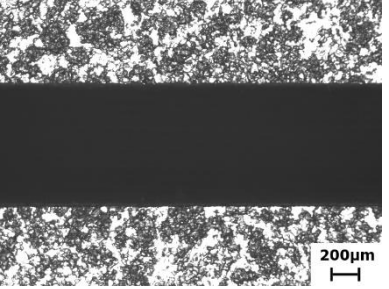
## 4 Results and discussion

### 4.1 Measured experimental $W_{top}$

The kerf width corresponding to different nozzle tip – focal point distance  $p_f$  is demonstrated on Table 6, where microscopic images of the top surface of the specimens cut with constant process parameters but varying  $p_f$  are presented. The values of the measured  $W_{top}$  data as a function of  $p_f$  collected from the experiment for threshold calibration is depicted on Fig. 7. It can be appreciated how the replicates of

each focus position have a  $W_{top}$  value contained in a small range showing the consistency of the measurement phase.

Table 6: Microscopic images of top surface of specimens cut with different  $p_f$ , displaying the kerf width

$T$ [mm]	3	5	8
Fixed parameters	$P = 6\text{ kW}$ $v = 2700\text{ mm/min}$ $p = 18\text{ bar}$ $SOD = 0.7\text{ mm}$	$P = 6\text{ kW}$ $v = 5600\text{ mm/min}$ $p = 18\text{ bar}$ $SOD = 0.7\text{ mm}$	$P = 6\text{ kW}$ $v = 3050\text{ mm/min}$ $p = 15\text{ bar}$ $SOD = 0.5\text{ mm}$
	$p_f = 2.40\text{ mm}$	$p_f = 3.60\text{ mm}$	$p_f = 5.00\text{ mm}$
			
	$p_f = 3.00\text{ mm}$	$p_f = 4.50\text{ mm}$	$p_f = 6.25\text{ mm}$
			
	$p_f = 3.60\text{ mm}$	$p_f = 5.40\text{ mm}$	$p_f = 7.50\text{ mm}$
			

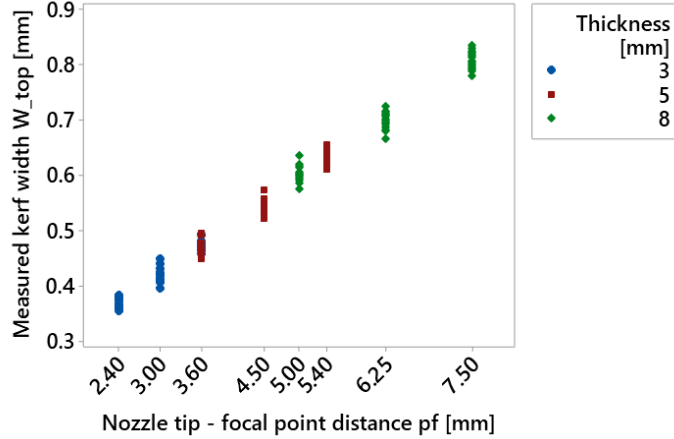


Fig. 7: Measured kerf width  $W_{top}$  as a function of the nozzle - focal point distance  $p_f$  considering all thicknesses

The statistical analysis of variance ANOVA (see Table 7: ANOVA table for  $W_{top}$  data) proves that the focal displacement  $p_f$  presents a significant factor influencing the kerf width value, rejecting the null hypothesis with a high significance of p-value equal to 0. Instead, the thickness of the material  $T$  exhibits p-value higher than the significance level of 0.05, thus retains the null hypothesis and is considered not statistically significant factor. Therefore, solely the nozzle tip – focal point distance  $p_f$  is considered hereafter as predictor in fitting the regression model for the kerf width estimation. The outliers were removed in the analysis.

Table 7: ANOVA table for  $W_{top}$  data

Source	DF	Adj SS	Adj MS	F-Value	P-Value
$p_f$	1	0.69407	0.69407	3826.54	0.000
$T$	1	0.00054	0.00054	2.97	0.087
Error	155	0.02811	0.00018		
Total	157	2.74131			

#### 4.2 Image analyses algorithm calibration

In the Subchapter 2.2., the procedure for analyzing the image data was thoroughly explained and the need for a proper threshold value to correctly distinguish between solid heated zone and actual molten material was justified. In Subchapter 2.3., the procedure for calibrating the threshold value was presented.

The results of the threshold value calibration are displayed on the plots on Fig. 8, where the error trend is described as a function of the threshold  $C$ . The variation of the square error of the measured  $W_{top}$  and the estimated kerf width  $W_{est}$  for different threshold values is calculated based on the relation Eq. 8, where  $M$  is the total number of cuts ( $M = 162$ ) and  $N$  is the total number of image frames considered per cut ( $N = 40$ ). The cut number is shown on the x-axis of the plots, which is set in a sequential order.

As defined,  $e_{TOT}$  is calculated as the sum of all square errors per cut divided by the total number of cuts. On Fig. 8 can be visualized that the lowest error value is achieved with a threshold of  $C = 7$  ( $e_{TOT} = 0.002$ ), implying that when using this threshold value for estimating the kerf width of a single frame, the correspondence of the kerf width  $W_{est}$  is most accurately correlated to the measured kerf width  $W_{top}$ . Even though threshold  $C = 8$  results in a reduced error for low thicknesses (case 3 mm and 5 mm), in the 8 mm case the error greatly increases. On the other hand, threshold  $C = 7$  spreads the error more evenly along all thicknesses, maintaining a low standard deviation of the error. As demonstrated, the optimal value of the threshold was found to be  $C = 7$ , and this value was employed for image analyses in the experimental campaign in order to have the closest estimation of  $W_{est}$  with respect to the measured  $W_{top}$ .



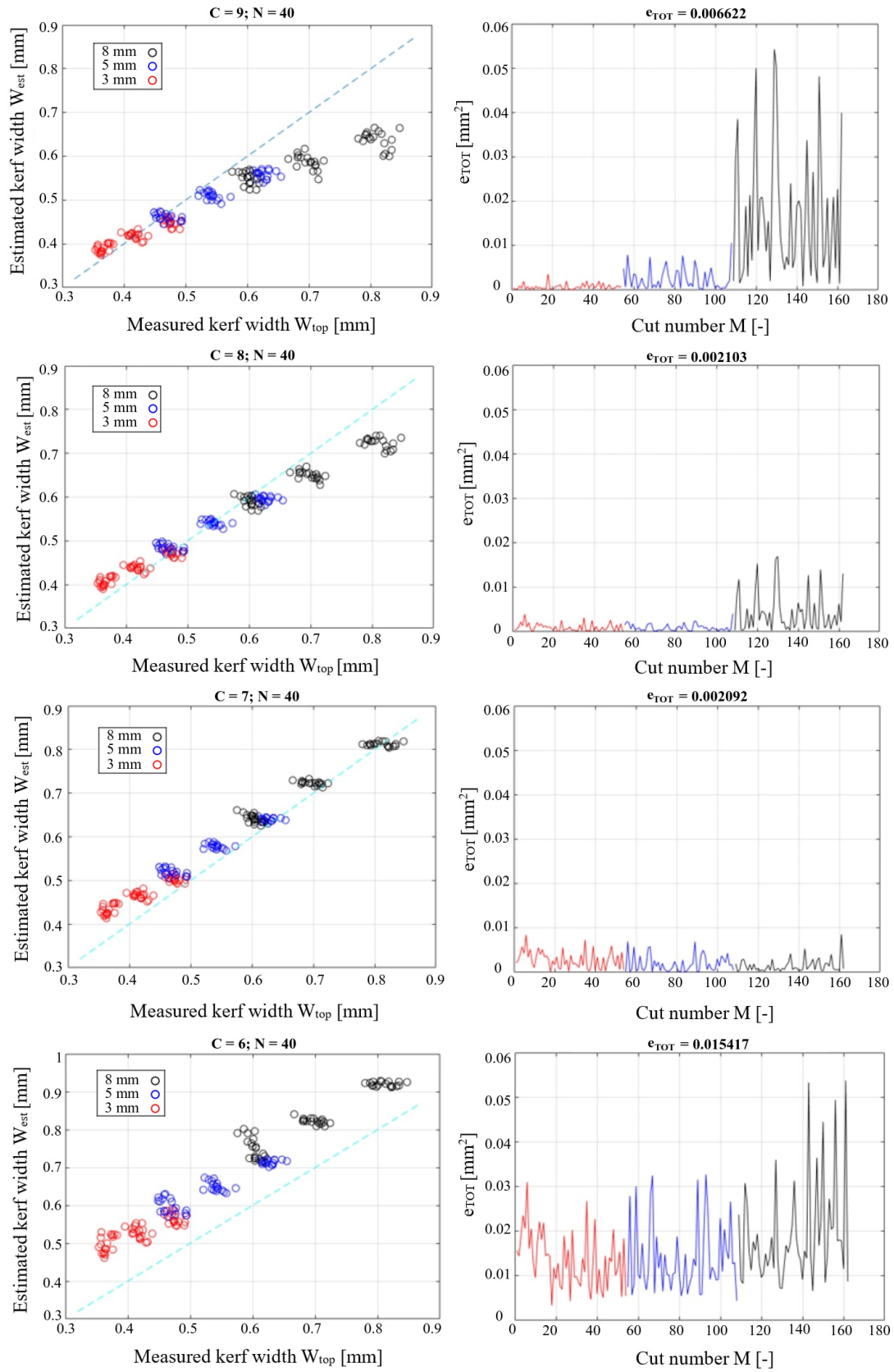


Fig. 8: Variation of the estimated kerf width  $W_{est}$  with respect to the measured kerf width  $W_{top}$  (left plots) and variation of the square error (right plots) for different threshold values

### 4.3 Process modelling

In previous paragraph, the statistical analysis of variance ANOVA showed that the kerf width variation is indubitably affected by the focal displacement, since the focus position rejected the null hypothesis with a high significance of p-value equal to 0. For this reason, a model which correlates the nozzle – focal point distance  $p_f$  and the estimated  $W_{est}$  from the acquired images can be fitted, with the aim of assessing the focus position variation. On Fig. 9, the averaged  $W_{est}$  from each cut of the experiment is plotted with respect to the corresponding  $p_f$  value used for that cutting condition. Only the data acquired during the stable region of the cut is used for analyses, therefore the data from the piercing and lead-on phase is not considered for process modelling. The standard deviation of the  $W_{est}$  is kept in small range confirming the stable cutting process. Furthermore, a linear regression model was developed, where the nozzle – focal point distance  $p_f$  was used as regressor and the estimated kerf width  $W_{est}$  as dependent variable. The linear fit is plotted on Fig. 9 where comparison between the experimental data and the fitted model is demonstrated. The model was found to fit the experimental data well with an accuracy of  $R_{adj}^2 \approx 99.22\%$  and P-value of lack-of-fit test equal to 0.24, while normality and homogeneity of the residuals were verified:

$$W_{est} = a + b \cdot p_f$$

Eq. 10

where  $a = 0.1927$  is the constant coefficient and  $b = 0,07091$  is the coefficient multiplying  $p_f$  in the regression equation.

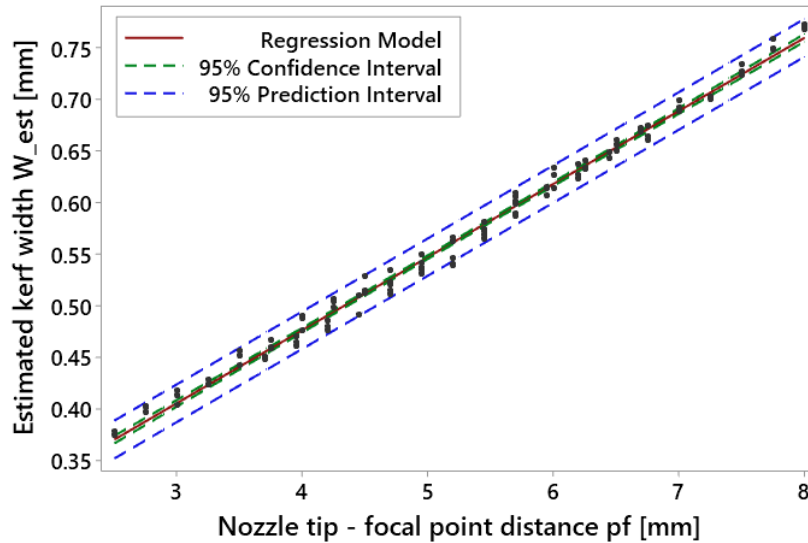


Fig. 9: Estimated kerf width  $W_{est}$  as a function of the nozzle - focal plane distance  $p_f$  with a comparison between experimental data and the fitted model. 95% confidence and prediction intervals are plotted.

To validate the regression curve and the data extraction algorithm, the measured kerf width data  $W_{top}$  gathered from the experimentation are plotted on Fig. 10, where it is visualized that most of the data points belong within the prediction interval, thus confirming the fitting of the regression model.

Furthermore, an estimation of the focus position is performed on a validation data subset by inserting the corresponding  $W_{est}$  values into the model equation on Eq. 10. The validation dataset consisted of five straight-line cuts on four different thicknesses (3, 4, 5 and 8mm), each cut performed with different  $p_f$  found within the range of the nozzle – focal plane distance per thickness listed on Table 4. The employed

fixed process parameters for each thickness are equal to the ones listed on Table 2. The model accurately estimated the focus position with a Mean Squared Error (MSE) of  $0.016 \text{ mm}^2$ .

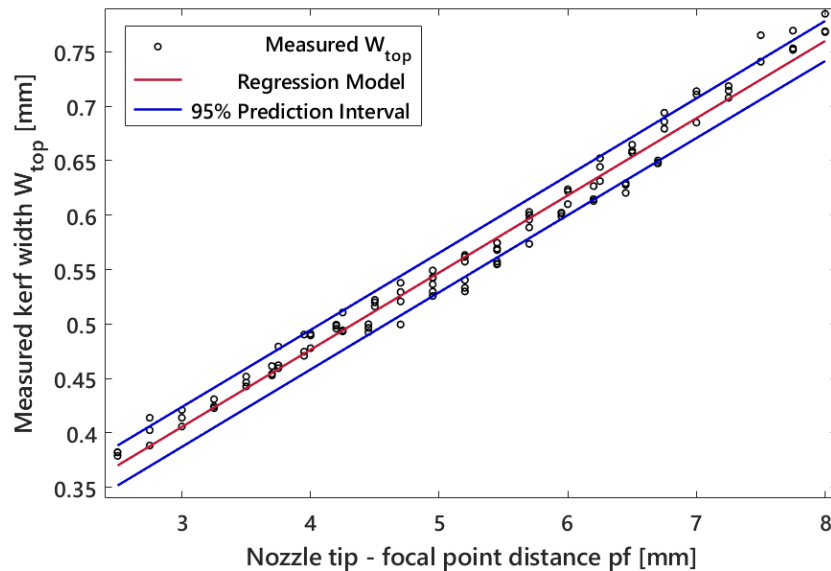


Fig. 10: Validation of the fitted regression model by plotting the measured kerf width data.

## 5 Conclusions

Measuring the kerf width of a straight-line cut with a microscope is a practical way to examine and adjust the focus position. With the aim of having a real-time observation of the kerf during the cutting process, a monitoring setup was mounted coaxially on the laser head, observing the thermal emission of the laser beam-material interaction. An image processing algorithm was developed to extract the kerf and derive its width from the acquired process images, providing an indirect method for estimating the generated kerf width. Results showed that by comparing the microscopically measured and the image-extracted kerf width, a proper threshold value can be found for binarizing the acquired image, such that an accurate estimation of the sensing signal is achieved. During stable cutting condition, the estimated kerf width remained constant. Furthermore, the capacitive sensor present on the laser head measures the *SOD*, thus any possible deformation of the sheet surface is compensated with a feedback loop maintaining a constant nominal *SOD*.

With the presented optical chain and process parameters, a theoretical range of  $\pm 1 \text{ mm}$  shift of the focus position from the nominal value was computed for a constant laser power. To simulate the focus shifting phenomenon, straight lines were cut each one performed with specific focus position within the evaluated range. Employing statistical analyses on the kerf width estimates, a regression model was fit on the experimental data, linearly relating the focus position and the kerf width with an 99.22% correspondence between the experimental data and the fitted model. The model is aimed to obtain a continuous real-time estimation of the focus position, by correlating the machine software with an external controller which will contain the image processing algorithms and the experimental model fit. Having the ability to quantify the focus shift while cutting gives the opportunity for open-loop control, when an alarm notifies excessive degradation of the optics, and for close-loop control, to mitigate small focus drift for defect avoidance. The real-time control will be a topic of further study.

The feasibility and practicality demonstrated by the solution presents one step closer to the “Intelligent machine” target of Industry 4.0. Furthermore, the discussed approach offers the advantage of aggregating

the influence of each optical element and providing the shift in focus position of the entire optical chain. Hence the resultant energy input on the laser-material interaction can be assessed, without the necessity to investigate and implement sensors on each optical element separately.

The present limitation of the solution is that simple cutting geometry was used where constant process parameters were employed. Cutting corners impose a change in the cutting speed. The superimposed influence of the cutting speed and focus position on the kerf width is a topic of future study. The presented work is addressed to point out a method, here experimentally tested on a common stainless steel and on the relative feasibility window of the process parameters when nitrogen inert laser cutting is used. This method may be extended to other materials and process conditions. However, when the material or the cutting method changes, a calibration of the value of the image threshold and the parameters of the regression model correlating  $p_f$  and  $W_{est}$  might be needed.

### Acknowledgements

The authors are grateful to Adige S.p.A. of the BLMGROUP for the professional support and the valuable and constructive suggestions about the laser cutting process received. The authors would also like to thank Gabriele Chini for the experimental works he provided during this study.

### Declarations

#### Funding

The project presented in this paper has been funded with the contribution of the Autonomous Province of Trento, Italy, through the Regional Law 6/99 (Project LT 4.0).

#### Conflict of interest

The authors declare that they have no known competing financial interests or personal relationships that could have appeared to influence the work reported in this paper.

#### Availability of data and material

The collected data required to reproduce the above findings cannot be shared at this time as the data is also used in an ongoing study.

#### Code availability

The codes used in the research work are available from the corresponding author upon reasonable request.

### References

- [1] S. Oh, I. Lee, Y. Bin Park, H. Ki, Investigation of cut quality in fiber laser cutting of CFRP, *Opt. Laser Technol.* 113 (2019) 129–140. <https://doi.org/10.1016/j.optlastec.2018.12.018>.
- [2] Y. Xing, L. Liu, Z. Wu, X. Wang, P. Huang, L. Tang, Fabrication and characterization of micro-channels on Al<sub>2</sub>O<sub>3</sub>/TiC ceramic produced by nanosecond laser, *Ceram. Int.* 44 (2018) 23035–23044. <https://doi.org/10.1016/j.ceramint.2018.09.106>.
- [3] S. Wadekar, S. U. Deokar, Effect of Process Parameters on Laser Cutting Process: A Review, *Imp. J. Interdiscip. Res.* 2(7) (2016) 434-439.
- [4] M. Sharifi, M. Akbari, Experimental investigation of the effect of process parameters on cutting region temperature and cutting edge quality in laser cutting of AL6061T6 alloy, *Optik (Stuttg.)*. 184 (2019) 457–463. <https://doi.org/10.1016/j.ijleo.2019.04.105>.

- [5] Y. Liu, Optimization of cutting parameters in machining, *Adv. Mater. Res.* 549 (2012) 871–874. <https://doi.org/10.4028/www.scientific.net/AMR.549.871>.
- [6] C. Karatas, O. Keles, I. Uslan, Y. Usta, Laser cutting of steel sheets: Influence of workpiece thickness and beam waist position on kerf size and stria formation, *J. Mater. Process. Technol.* 172 (2006) 22–29. <https://doi.org/10.1016/j.jmatprotec.2005.08.017>.
- [7] T. ARAI, Generation of Striations During Laser Cutting of Mild Steel, *SOP Trans. Appl. Phys.* 2014 (2014) 81–95. <https://doi.org/10.15764/aphy.2014.02010>.
- [8] M.H. Mahdieh, H. Moradi, Experimental and Theoretical Investigations of Beam Deformation Produced by Thermal Lens Effect on a Gaussian Laser Beam in Ethanol, *Lasers Manuf. Mater. Process.* (2020). <https://doi.org/10.1007/s40516-020-00116-0>.
- [9] L. Tatzel, F.P. León, Impact of the thermally induced focus shift on the quality of a laser cutting edge, *J. Laser Appl.* 32 (2020) 022022. <https://doi.org/10.2351/7.0000053>.
- [10] S. Eiselen, H. Zapf, E. Mantel, L. Hofmann, M. Schmidt, Impact of thermal focal shift on laser cutting processes with high brightness lasers, *ICALEO 2012 - 31st Int. Congr. Appl. Lasers Electro-Optics.* 282 (2012) 282–291. <https://doi.org/10.2351/1.5062458>.
- [11] F. Nagel, A. Patschger, J.P. Bergmann, J. Bliedtner, Investigations on the active compensation of the focal shift in scanning systems using a temperature signal, *Appl. Opt.* 57 (2018) 3561. <https://doi.org/10.1364/ao.57.003561>.
- [12] M. Liu, B. Li, Y. Wang, H. Hao, Measuring surface deformation of optical components with surface thermal lens technique, *Laser-Induced Damage Opt. Mater.* 2008. 7132 (2008) 71320T. <https://doi.org/10.1117/12.804175>.
- [13] B. Neumeier, D. Schmitt-Landsiedel, Online condition measurement of high power solid state laser cutting optics using ultrasound signals, *Phys. Procedia.* 56 (2014) 1252–1260. <https://doi.org/10.1016/j.phpro.2014.08.041>.
- [14] R.L. Byer, Deformable Mirrors for High-Power Lasers, 4493 (2002) 55–63.
- [15] G. Eberle, V. Chiron, K. Wegener, Simulation and realization of a focus shifting unit using a tunable lens for 3D laser material processing, *Phys. Procedia.* 41 (2013) 441–447. <https://doi.org/10.1016/j.phpro.2013.03.100>.
- [16] K. Mann, B. Schäfer, M. Stubenvoll, K. Hentschel, M. Zenz, Measurement and compensation of wavefront deformations and focal shifts in high-power laser optics, *Laser-Induced Damage Opt. Mater.* 2015. 9632 (2015) 96321D. <https://doi.org/10.1117/12.2196160>.
- [17] M.S. Roth, T. Graf, H.P. Weber, End-pumped Nd:YAG laser with self-adaptive compensation of the thermal lens, *Conf. Lasers Electro-Optics Eur. - Tech. Dig.* 190 (2003) 41. <https://doi.org/10.1109/CLEOE.2003.1312103>.

- [18] M. Scaggs, G. Haas, Thermal lensing compensation optics for high power lasers, *Laser Reson. Beam Control XIII*. 7913 (2011) 79130C. <https://doi.org/10.1117/12.871370>.
- [19] P. Herwig, U. Klotzbach, M. Walther, J. Hauptmann, A. Wetzig, E. Beyer, Aberrations induced by high brightness lasers, *Phys. Procedia*. 12 (2011) 779–786. <https://doi.org/10.1016/j.phpro.2011.03.097>.
- [20] M. Hemmerich, C. Thiel, F. Lupp, H. Hanebuth, R. Weber, T. Graf, Reduction of focal shift effects in industrial laser beam welding by means of innovative protection glass concept, *Phys. Procedia*. 56 (2014) 681–688. <https://doi.org/10.1016/j.phpro.2014.08.161>.
- [21] F. Abt, A. Hess, F. Dausinger, Temporal behaviour of the focal shift of beam forming optics for high power single mode lasers, *ICALEO 2008 - 27th Int. Congr. Appl. Lasers Electro-Optics, Congr. Proc.* 1302 (2008) 561–568. <https://doi.org/10.2351/1.5061242>.
- [22] A. Optics, 2020 APPLIED OPTICS / Vol. 15, No. 9 / September 1976, 15 (2020) 2020–2022.
- [23] J.-P. Negel, F. Abt, D. Blázquez-Sánchez, A. Austerschulte, M. Hafner, T. Liebig, P. von Strobl-Albeg, R. Weber, M. Abdou Ahmed, A. Voss, T. Graf, Controlling the thermally induced focal shift in laser processing heads, *High Power Laser Mater. Process. Lasers, Beam Deliv. Diagnostics, Appl.* 8239 (2012) 823911. <https://doi.org/10.1117/12.906634>.
- [24] D. Reitemeyer, T. Seefeld, F. Vollertsen, Online focus shift measurement in high power fiber laser welding, *Phys. Procedia*. 5 (2010) 455–463. <https://doi.org/10.1016/j.phpro.2010.08.073>.
- [25] H. Haferkamp, M. Goede, A. von Busse, <title>Quality monitoring and assurance for laser beam cutting using a thermographic process control</title>, *Opt. Meas. Syst. Ind. Insp.* 3824 (1999) 383–391. <https://doi.org/10.1117/12.364276>.
- [26] U. Thombansen, T. Hermanns, S. Stoyanov, Setup and maintenance of manufacturing quality in CO<sub>2</sub> laser cutting, *Procedia CIRP*. 20 (2014) 98–102. <https://doi.org/10.1016/j.procir.2014.05.037>.
- [27] W. Weingartner, K. Schröder, D. Schuöcker, System for monitoring the focal position in laser material processing, *Appl. Opt.* 40 (2001) 4297. <https://doi.org/10.1364/ao.40.004297>.
- [28] E. V. Bordatchev, S.K. Nikumb, Effect of focus position on informational properties of acoustic emission generated by laser-material interactions, *Appl. Surf. Sci.* 253 (2006) 1122–1129. <https://doi.org/10.1016/j.apsusc.2006.01.047>.
- [29] M. Pacher, L. Mazzoleni, L. Caprio, A.G. Demir, B. Previtali, Estimation of melt pool size by complementary use of external illumination and process emission in coaxial monitoring of selective laser melting, *J. Laser Appl.* 31 (2019) 022305. <https://doi.org/10.2351/1.5096117>.
- [30] M. Pacher, L. Franceschetti, S.C. Strada, M. Tanelli, S.M. Savaresi, B. Previtali, Real-time continuous estimation of dross attachment in the laser cutting process based on process emission images, *J. Laser Appl.* 32 (2020) 042016. <https://doi.org/10.2351/7.0000145>.

- [31] I. Miyamoto, H. Nanba, H. Maruo, Analysis of Thermally Induced Optical Distortion in Lens during Focusing High Power CO<sub>2</sub> Laser Beam, Proc. SPIE. 1276 (1990) 112–121.
- [32] S. Rummel, G. Herriot, A. Hedges, Comparison of 1 micron transmissive optical materials for high power lasers, 29th Int. Congr. Appl. Lasers Electro-Optics, ICALEO 2010 - Congr. Proc. 103 (2010) 21–28. <https://doi.org/10.2351/1.5062029>.
- [33] W. M. Steen and J. Mazumder, Laser Material Processing (Springer, London, 2010)